Meas. Sci. Technol. **18** (2007) 2972–2978 doi:10.1088/0957-0233/18/9/030

A beam-deflection probe as a method for optodynamic measurements of cavitation bubble oscillations

Rok Petkovsek, Peter Gregorcic and Janez Mozina

Faculty of Mechanical Engineering, University of Ljubljana, Aškerčeva 6, SI-1000 Ljubljana, Slovenia

E-mail: rok.petkovsek@fs.uni-lj.si

Received 10 May 2007, in final form 13 June 2007
Published 10 August 2007
Online at stacks.iop.org/MST/18/2972

Abstract
High-intensity light from a laser pulse can produce laser-induced breakdown in a liquid followed by a shock wave and the growth of a cavitation bubble. When the bubble reaches its maximum radius, the pressure of the surrounding liquid causes it to collapse; this results in bubble oscillations. The cavitation bubble's oscillations and the corresponding shock waves were measured from the deflections of a laser beam. These deflections were detected using a fast quadrant photodiode, built into the optical probe. The precise relative-positioning system and the small diameter of the beam's waist made it possible to detect and analyse the signals from the shock wave and the cavitation bubble. Here, we have demonstrated that a method based on a beam-deflection probe can be used to measure the fast phenomena that follow immediately after laser-induced breakdown as well as the whole dynamics of the bubble oscillations, which corresponds to a three-orders-of-magnitude larger time scale.

Keywords: optodynamics, beam-deflection probe, non-contact measuring, cavitation bubble, shock wave, laser-induced breakdown

1. Introduction

A high-intensity laser pulse ($>10^{14}$ W m^{-2}) in the ns range that is focused into distilled water will induce optical breakdown, i.e., the partial or complete ionization of the liquid media, resulting in a plasma—a 'gas' of charged particles [1]. Such a plasma is a strong absorber of the light from the laser pulse and is thus rapidly heated to $\sim 10^4$ K, while the pressure increases to as high as 10^5 bar [2]. An explosive expansion followed by the appearance of an optically induced plasma represents a typical optodynamic process, in which the energy of the laser is converted into the mechanical energy of the liquid medium, determined by dynamic phenomena, i.e., the propagation of a shock wave and the growth of a cavitation bubble. When the cavitation bubble reaches its maximum extent the process begins to reverse; due to the pressure of the surrounding liquid the radius of the bubble starts to decrease, and finally it collapses. This collapse, in turn, initiates a new cycle of bubble growth and bubble collapse. The process therefore repeats itself, resulting in the so-called cavitation-bubble oscillations, with a new shock wave being emitted after every collapse.

There are several optical methods for detecting and measuring cavitation bubbles and shock-wave fronts, such as high-speed photography [3–5], shadow photography [2, 6, 7], schlieren photography [4, 8], streak photography [8, 9], holograph-based photography [10, 11], a laser beam-deflection probe (BDP) [4, 12, 13] and combinations of these methods. Electromechanical detectors (such as a hydrophone) have also been used [14, 15] as an independent measurement method or in combination with one of the optical techniques. However, the very high pressure of the shock wave in the vicinity of the breakdown region limits their application due to their relatively low damage threshold. This means that electromechanical sensors are appropriate for far-field measurement, but they are inappropriate for measurements of bubble dynamics.

When choosing a measuring process that has good repeatability for the case of a laser-induced cavitation bubble,

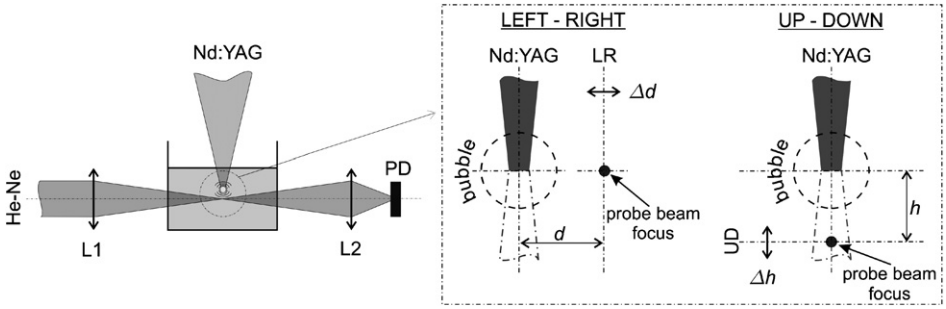

Figure 1. Experimental setup. Left: He–Ne laser, used as a probe beam, was led through the lens (L1, L2) onto the fast positioning photo-detector (PD). Breakdown was induced by a pulsed Nd:YAG laser. Right: sketch of the probe-beam positions during the bubble scanning in the vertical (left–right) and horizontal (up–down) directions.

shadow photography probably represents the most commonly used method, due to its relative simplicity. In principle, its time resolution depends only on the pulse duration of the light source. Like the shadow-photography method, the technique based on the laser BDP also requires a relatively simple experimental setup. The main differences between the two methods are as follows. With shadow photography the whole 2D image of the bubble can be observed at once. However, measuring the evolution over time requires the repetition of the process or very sophisticated equipment. In contrast, with the laser BDP the whole time evolution of the bubble can be measured using a single shot, but only at one point in space. Therefore, from a single laser BDP measurement signal information on bubble expansions and collapses resulting in oscillations and the corresponding shock waves can be obtained. Furthermore, by using a scanning procedure the dynamic behaviour in 1D or 2D can also be measured; however, this requires sufficient process repeatability.

Measurements based on the BDP technique are possible because plasmas, shock waves and cavitation bubbles locally change the refractive index. When these disturbances cross the path of the probe, the refractive-index gradient results in a measurable deflection of the probe beam [16–18], and these beam deflections can be detected with a position-sensing photo-detector such as a quadrant photodiode. In this paper we describe the application of a laser BDP as a non-contact, sensitive and precise measuring device for the detection of cavitation bubble dynamics as well as the corresponding shock waves. This sort of probe can be used in various applications, such as shock-wave [12] and plasma characterization [19], an optical investigation of laser-drilling mechanisms [13], measurements of the energy-conversion efficiency during laser ablation [20] or monitoring of the laser drilling of through-holes in glass ampoules used in the pharmaceutical industry [21].

For the breakdown formation we applied a Q-switched Nd:YAG laser, focused into a vessel that was filled with distilled water. A suitably designed positioning system for moving the laser probe beam relative to the optical axis and the focus of the breakdown laser made it possible to carry out one- or two-dimensional scanning of the cavitation bubble. The software, developed in Matlab, made it possible to automatically control the experiment, the data acquisition and the data processing.

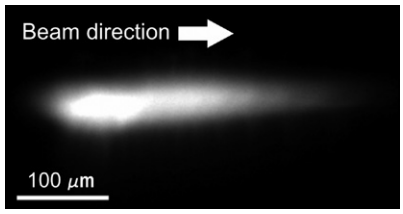

Figure 2. Plasma in distilled water induced by a 7 ns laser pulse with an energy of 8.6 mJ.

2. Experimental setup

2.1. Breakdown laser and breakdown threshold

The breakdown in water was induced by a laser pulse that was focused into the vessel containing the distilled water, as shown in figure 1. In our experiments we used a Q-switched Nd:YAG laser ($\lambda = 1064$ nm), designed for ocular photo-disruption. The laser has an energy attenuator that gave us the ability to operate at ten different energies. Most of the experiments presented in this paper were made at one of the three laser energies: $8.6 \times (1 \pm 0.03)$ mJ, $6.0 \times (1 \pm 0.03)$ mJ and $2.41 \times (1 \pm 0.03)$ mJ. An attenuator was placed in front of the laser optics, ensuring that the beam characteristics did not depend on the position. Since the duration of the laser pulse was 7 ns, the power of the laser pulses was in the range of 0.3–1.2 MW.

The beam waist of the breakdown laser in water was estimated from a crater radius made in a piece of metal, positioned at the focus of the laser. The crater was made at the lowest energy of the laser pulse (0.39 mJ) and its radius was measured with a microscope. The estimated beam radius at the focus was $\sim$30 μm. The intensities used in the experiment were therefore in the range of $1–4 \times 10^{14}$ W m^{-2}.

When the intensity of a laser pulse that is focused into water reaches or exceeds threshold intensity, I_{th}, breakdown occurs in the focal region. First, a plasma is generated at the focus, which then expands towards the incoming beam. Strong absorption of the laser light in the plasma then blocks the light from the laser pulse, resulting in plasma shielding [22]. A plasma in distilled water made with a laser energy of 8.6 mJ is shown in figure 2. Distilled water was used in order to provide reproducible experimental conditions. The breakdown threshold was measured by counting the frequency of the plasma-lighting occurrences. A total of

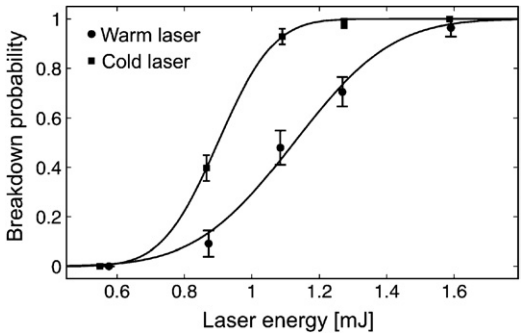

Figure 3. Breakdown probability versus breakdown laser-beam energy for distilled water. Measurements were made for the case of cold (squares) and warm (points) lasers. The Gaussian error function fitted to the measured data is represented by a solid line. The threshold energy, E_{th}, corresponds to a 50% breakdown probability.

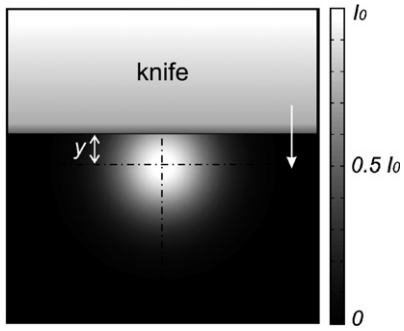

Figure 4. Cross-section of the Gaussian beam (xy-plane) when using the knife-edge method.

30–80 measurements were made for each energy value, with the breakdown being detected by a photodiode. A trigger value was set for the photodiode signal values corresponding to plasma lighting detected with the naked eye in a dark room. The breakdown probability was plotted as a function of the laser energy, E_l, and the Gaussian error function was fitted to the measured data (figure 3). For the threshold energy, E_{th}, we chose a value that corresponds to a 50% breakdown probability, as is suggested in [23].

Measuring the laser energy instead of the beam intensity requires a constant radius of the beam focus. However, when our laser warmed up, a temperature gradient appeared in the amplification medium. The type of laser we used does not have active cooling, because in intraocular laser treatments, typically only a few successive pulses are used to perform the procedure. This temperature gradient in the amplification medium affects the beam quality, and as a result, the laser intensity decreases and the energy threshold, E_{th}, increases. The phenomenon is demonstrated in figure 3, where measurements for a cold and a warm laser are plotted. We defined the laser as being cold when the time between measurements with a single energy value exceeded 30 min. For the threshold energy during all our measurements we considered the value corresponding to the warm laser, i.e., $E_{\text{th}} = 1.1 \times (1 \pm 0.1)$ mJ.

2.2. Beam-deflection probe

The experimental setup for the laser BDP is shown in figure 1. The breakdown was achieved by focusing the Nd:YAG laser into the vessel containing distilled water. The breakdown was detected by the photodiode that we also used as a trigger for the BDP signal acquisition. The BDP consists of a probe beam and a fast quadrant photodiode.

A He–Ne laser ($\lambda = 633$ nm) was used as the probe beam. The temporal resolution and the frequency bandwidths of the probe were determined by the photo-detector and the corresponding electronic circuit as well as by the probe beam's waist diameter. In order to achieve a small diameter of the beam at the focal point, it was first expanded and then focused through the lens L1 into the vessel. The beam was then led through the lens L2 in front of the fast quadrant photodiode, built into the optical probe. The waist radius of the probe beam was approximately ~ 3 μm, and by considering the speed of sound in water this roughly corresponds to the rise time of the detector (4 ns). The beam-waist radius was measured using the standard knife-edge method. The estimated M^2 beam-quality factor for the applied probe beam was $M^2 \sim 1.1$.

Precise measurements using a BDP require that the optical axis of the breakdown laser lies in the focal plane of the probe beam (see also the right-hand side of figure 1). In order to solve the problem relating to the accurate positioning of the breakdown in the focal plane of the probe, we developed a system for beam positioning based on a combination of the knife-edge method and time-of-flight measurements using the quadrant photo-diode. The same system was also used for the beam-parameter measurements.

In general, laser-beam propagation can be approximated by an ideal Gaussian intensity profile, corresponding to the theoretical TEM_{00} described by the equation:

$$I(x, y, z) = I_0 \frac{w_0^2}{w^2(z)} \, \mathrm{e}^{-2\frac{x^2+y^2}{w^2(z)}}. \tag{1}$$

Here, w_0 denotes the beam-waist radius, I is the intensity at any point, I_0 is the intensity in the centre of the beam focus, x and y are coordinates in the transverse plane and z is the coordinate along the beam. Transmitted power versus total power in dependence of knife position, y (figure 4), can therefore be calculated as

$$\frac{P_y}{P_{\text{tot}}} = \frac{\int_{-\infty}^{\infty}\int_{-\infty}^{y} I(x, y', z)\,\mathrm{d}x\,\mathrm{d}y'}{\int_{-\infty}^{\infty}\int_{-\infty}^{\infty} I(x, y, z)\,\mathrm{d}x\,\mathrm{d}y} = \frac{1}{2}\left[1 + \operatorname{erf}\left(\frac{\sqrt{2}y}{w(z)}\right)\right]. \tag{2}$$

While the laser beam travels through the optical elements, in reality it is not a true Gaussian beam. A quality factor, $M^2 > 1$, is normally used to describe the deviation of the real beam from the Gaussian beam. If w and ϑ denote the waist radius and far-field divergence of an ideal beam respectively, the beam quality factor, M^2 is defined as:

$$M^2 = \frac{w_{0r}\vartheta_r}{w_0\vartheta}, \tag{3}$$

where w_{0r} and ϑ_r are the beam-waist radius and far-field divergence of the real beam, respectively. The beam quality factor, M^2, tells us the ratio between the real and the ideal beam-waist radius if both have a radius r for a lens with a focus f.

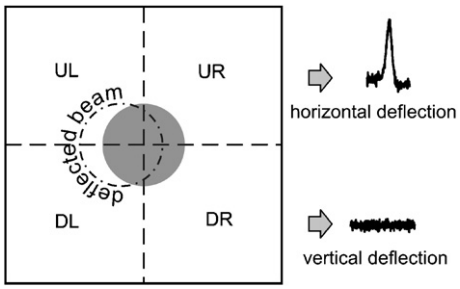

Figure 5. Sketch of the quadrant photodiode and the probe beam, deflected only in the horizontal direction. The signals for this case are shown on the right.

The real beam radius at the z-coordinate can therefore be represented as

$$w(z) = w_{0r}\sqrt{1 + \frac{M^2\lambda^2 z^2}{\pi^2 w_{0r}^2 n^2}}, \tag{4}$$

where λ and n are the wavelength of the laser light and the refractive index of the medium, respectively.

Software based on the theory describing real-beam propagation was developed and implemented in the experimental system and enabled us to measure automatically the beam-waist radius, its position and the beam quality factor. The beam-waist radius was calculated by fitting equation (2), while the beam quality factor and waist position were deduced from measurements and by fitting equation (4), which describes real-beam propagation, to the measured data.

The probe-beam deflections in the directions 'left–right' and 'up–down' were measured using the fast quadrant photodiode, as is schematically shown in figure 5. Two signals obtained from the detector were used: the first one is proportional to the difference between the intensities in the upper and the lower quadrants (UL+UR)−(DL+DR), while the second one is proportional to the difference between the intensities in the left- and the right-hand quadrants (UL+DL)−(UR+DR) (figure 5). Therefore, the first signal corresponds to beam deflections in the vertical direction, while the second signal corresponds to beam deflections in the horizontal direction. By analysing both the signals, the relative position in two dimensions related to the breakdown region can be obtained. The estimated rise time and the bandwidth of the quadrant photodiode are ∼4 ns and ∼200 MHz, respectively and to the best of our knowledge, this is the fastest photo-detection system based on quadrant photodiode employed in a laser BDP probe.

2.3. The measuring method

The shock wave and the cavitation bubble that result from the breakdown caused by the Nd:YAG laser were detected with the laser BDP. A shock wave locally changes the density of water, which in turn causes a change in the refractive index [16], while in the case of the cavitation bubble, the refractive index is changed in the bubbles wall, which represents the border between the liquid and the vapour [24]. The refractive-index gradient results in a deflection of the probe beam [16–18]. The measurements presented in this paper were made by scanning in one dimension, perpendicular to the optical axis of the breakdown laser. The scanning procedure had to be performed in a direction perpendicular to the cavitation bubble wall propagations in order to obtain its velocity. Therefore the setup had to be precisely aligned. This was done by observing both the signals corresponding to the vertical and the horizontal deflections of the probe beam, respectively. Because we applied horizontal scanning (i.e., perpendicular to the breakdown beam direction), the horizontal deflections (see figure 5) represented our useful signal. On the other hand, the signal corresponding to the vertical deflections was observed in order to align the setup. When the horizontal scanning direction was perfectly parallel to the cavitation bubble propagation, there was no deflection in the vertical direction. Typical scannings were performed by utilizing a 30 μm shift of the probe beam. The cavitation bubble dynamics was measured at three different values of the breakdown laser energy: $E_{l1} = 8.6 \times (1 \pm 0.03)$ mJ, $E_{l2} = 6.0 \times (1 \pm 0.03)$ mJ and $E_{l3} = 4.7 \times (1 \pm 0.03)$ mJ, corresponding to $\beta_1 = 7.8 \pm 1$, $\beta_2 = 5.5 \pm 0.7$ and $\beta_3 = 4.2 \pm 0.6$. Here, β is the normalized laser-pulse energy, $\beta = E/E_{\text{th}} = I/I_{\text{th}}$ [22].

The scanning system used for changing the distance between the breakdown region and the probe-beam focus made possible a 1 μm shift. In the case of 30 μm shifts the error was estimated to be ± 1 μm. For each position of the probe beam up to five measurements were made, while the time between the consecutive measurements was about 10 s, which was necessary in order to allow adequate cooling of the breakdown laser. Furthermore, this time interval between each measurement is required to avoid the small gas bubbles that remain in the focal region for a few seconds after the breakdown occurs and may change the intensity threshold I_{th} [23].

The signals from the quadrant photodiode were observed with a digital oscilloscope (500 MHz Wave Runner 6050A, LeCroy), which was triggered by the signal from the diode detecting the plasma-light emission. The breakdown laser energy was also measured automatically during the experiments, and software was developed for the computer control of the experiment, the data acquisition and the data processing.

3. Results and discussion

The measurements were performed by scanning in the horizontal direction, perpendicular to the optical axis of the breakdown laser. It means that the probe beam was deflected in the horizontal direction only, as is schematically shown in figure 5. Figure 6 shows a typical signal from the beam-deflection probe corresponding to the horizontal deflection; it represents a shock wave and a cavitation bubble when the probe beam is positioned at $d = 200$ μm and $h = 0$ μm (see the right-hand side of figure 1) from the breakdown region. The energy of the breakdown laser was 8.6 mJ ($\beta = 7.8$). Peaks 1, 2, 3 and 4 correspond to the shock wave, while peak 5 corresponds to the cavitation bubble during its expansion. It is important to note that the positive peaks in figure 6 correspond to deflections away from the centre of the breakdown region that represents the source of the shock-wave front and the cavitation bubble. The negative peaks correspond to deflections towards the centre. The magnitude of the deflections at the photodiode

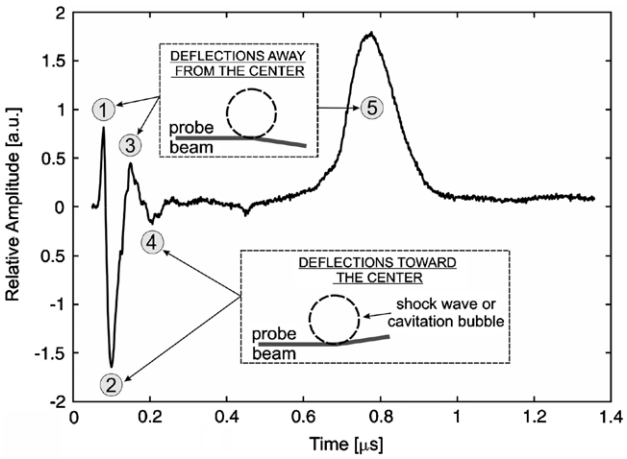

Figure 6. Typical BDP signal showing a shock wave and a cavitation bubble. Peak 1 corresponds to the beam reflection from the surface of the shock-wave front, while peaks 2, 3 and 4 correspond to known effects: the high pressure gradient of the shock front, the diverging lens effect and the presence of the rarefaction wave. Peak 5 corresponds to the cavitation bubble during its expansion. Two insertions in the figure show the direction of the probe beam deflection relative to the centre of a shock wave front and a cavitation bubble.

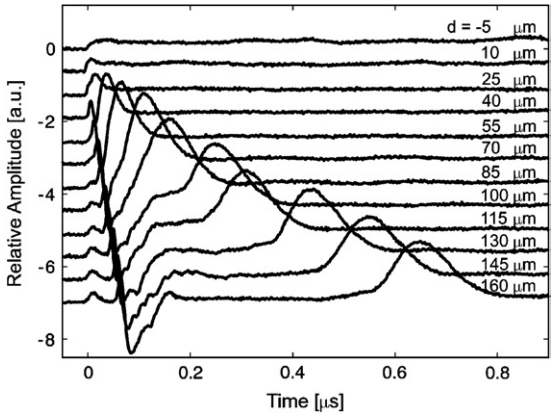

Figure 7. Shock-wave and cavitation-bubble separation immediately after breakdown. The signal sequence corresponds to a total BDP shift of 165 μm; thus two consecutive signals from the graph correspond to a shift of 15 μm. The first signal from the graph corresponds to the BDP position at the centre of the breakdown.

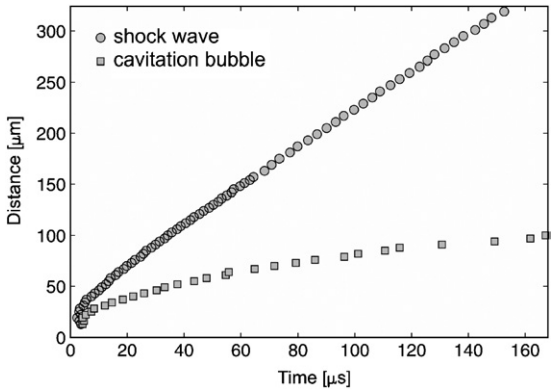

Figure 8. Time of flight for a shock wave (circles) and a cavitation bubble (squares) immediately after breakdown. Each point on the graph represents an average of five measurements.

for the applied BDP system was up to 2 mm. For example, for peaks 1, 2, 3, 4, 5 from figure 6, the deflection magnitudes on the photo-detector correspond approximately to 0.4, 1.1, 0.2, 0.1 and 1 mm, respectively. We observed that the amplitude of peak 1 depends strongly on the diameter of the probe beam; it decreases with increasing diameter and/or in the case when the breakdown position is shifted (in the z-direction) from the probe beam's focal plane. This leads us to the assumption that peak 1 appears because the probe beam is partially reflected (away from the centre) from the surface of the pressure front representing the shock wave. After peak 1, a rapid fall appears (peak 2) because the high-pressure part of the shock front crosses the probe beam's path. Peak 3 is caused by a deflection resulting from the diverging lens effect, similar to that obtained with a thin-walled tube, while peak 4 represents a negative deflection caused by the presence of a rarefaction wave [16]. It is also clear that the signal due to the transition of the cavitation bubble's wall is wider than the signal due to the shock wave; the main reason being that the shock wave is already much faster than the cavitation bubble at this distance (200 μm). Peaks 2, 3 and 4 represent the main characteristics of the shock-wave response curve, already described in [16], while the occurrence of the first peak, to the best of our knowledge, was not reported before. The main reason for this lies probably in the radius of the probe beam's waist and/or the breakdown position (in the z-direction) relative to the probe beam's focal plane.

Immediately after breakdown the water in the focal region is in the supercritical state ($T \gg T_{\mathrm{crit}} = 374\ ^{\circ}\mathrm{C}$, $p \gg p_{\mathrm{crit}} = 22.5$ MPa), and therefore at the early stage of a plasma expansion all phenomena (plasma, shock wave and cavitation bubble) coexist within the boundary between the supercritical water and the water under normal conditions. The plasma expansion proceeds with a pressure and temperature drop leading to the supercritical water forming steam. At that moment a phase boundary develops between the steam and the surrounding liquid, and from then on it is possible to talk in terms of the existence of a cavitation bubble [24]. Typical signals corresponding to the separation of the shock wave and the cavitation bubble (for a breakdown laser energy of 8.6 mJ, $\beta = 7.8$) are shown in figure 7. The sequence of signals corresponds to a total BDP shift of 165 μm; thus two consecutive signals from the graph correspond to a shift of 15 μm. The first signal from the above corresponds to the BDP positioned in the centre of the breakdown. Consequently, there is almost no deflection of the beam. In figure 8 the times of flight for a shock wave (circles) and a cavitation bubble (squares) are shown. It is clear that during the early stages of optodynamic phenomena a shock wave and a cavitation bubble coexist and therefore they cannot be distinguished, while later on the shock wave propagates much faster than the cavitation bubble's wall. Each point on the graph represents an average of five measurements.

A typical signal, including all the peaks we observed with the beam-deflection probe, is shown in figure 9. In this case the energy of the breakdown laser was 4.7 mJ ($\beta = 4.3$), and the distance between the breakdown region and the BDP optical axis was ~400 μm. Soon after the breakdown ($t \sim 0.5$ μs)

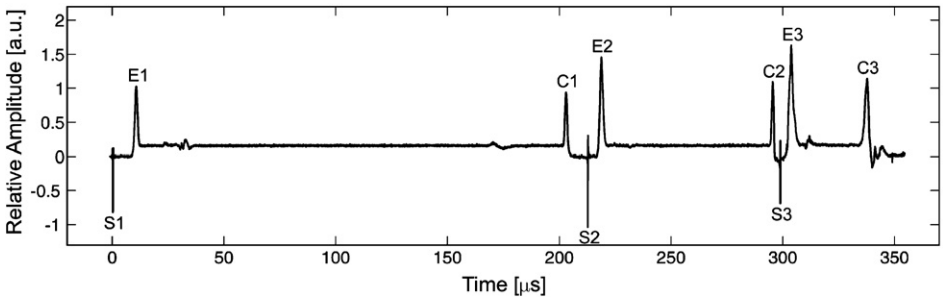

Figure 9. Typical signal including all the peaks observed with the BDP for a breakdown laser energy of 4.7 mJ and a distance between the breakdown region and the BDP optical axis of ∼400 μm. Peaks E1, E2 and E3 correspond to the bubble's expansions and the peaks C1, C2 and C3 correspond to the bubble's collapses. Peak S1 represents the first shock wave, caused by the breakdown, while peaks S2 and S3 correspond to secondary shock waves resulting from the bubble's collapses.

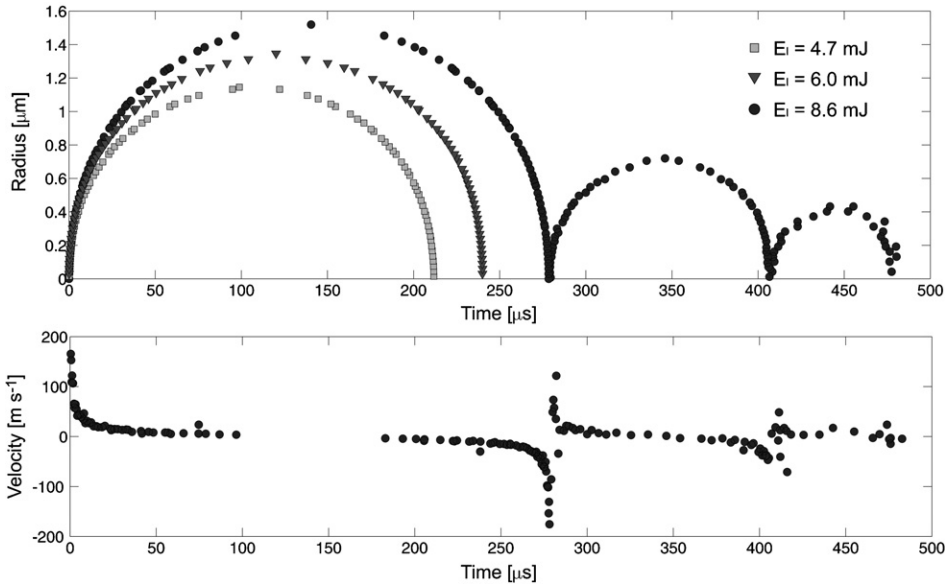

Figure 10. Bubble radius versus time for three breakdown laser energies (8.6 mJ, 6.0 mJ and 4.7 mJ). Three oscillations are shown for the maximum laser energy, while for the other values of the laser energy only the first oscillation is shown, to avoid a lack of clarity. Bottom: velocity of the bubble wall corresponds to $E_l = 8.6$ mJ.

the first peak S1 appears, represented in the shock wave described above. The following peak, E1, shows the cavitation bubble during its expansion. After the maximum radius is reached the cavitation bubble starts to collapse due to pressure from the surrounding liquid. Therefore, the bubble wall crosses the probe beam once again after ∼200 μs (peak C1). After the collapse a new shock wave is emitted. This is also observed with the BDP (peak S2). The oscillations are repeated several times and are detected as the peaks E2 and E3, representing the second and third expansions of the cavitation bubble and as peaks C2 and C3, representing its collapses. A third shock wave caused by a second collapse (peak S3) was also detected.

A quantitative evolution of the measured cavitation bubble's radius is shown in figure 10. The vertical axis represents the bubble radius and corresponds to the position of the probe beam relative to the breakdown site (i.e., cavitation bubble source) during the scanning procedure. The time for each particular radius was obtained from the beam deflection signal corresponding to the current position of the probe beam. Peaks E1, C1, E2, C2, E3 and C3 (e.g., see figure 9) of each signal correspond to the time of flight of the cavitation bubble wall during its first, second and third expansions and collapses, respectively. The data presented in figure 10 were statistically processed. Three oscillations are shown for the maximum laser energy (8.6 mJ, $\beta = 7.8$), while for other values of the laser energy (6.0 mJ, $\beta = 5.5$ and 4.7 mJ, $\beta = 4.3$) only the first oscillation is shown, in order to avoid a lack of clarity. The velocity of the bubble wall for the maximum laser energy ($\beta = 7.8$), which can be deduced from the slope of the radius versus time curve, is also shown at the bottom of figure 10.

The measured radii for the first oscillation were: 1.55 ± 0.06 mm, 1.34 ± 0.06 mm and 1.17 ± 0.06 mm for laser pulse energies $E_l = 8.6$, 6.0 and 4.7 mJ, respectively. Results are in accordance with results from Brujan *et al* [15]. In addition, we also measured the second and the third oscillations. Maximum radii for the second oscillation were: 0.68 ± 0.04 mm, 0.59 ± 0.04 mm and 0.48 ± 0.04 mm, while maximum radii for the third oscillation were: 0.39 ± 0.03 mm, 0.32 ± 0.03 mm and 0.25 ± 0.03 mm, for laser pulse energies $E_l = 8.6$, 6.0 and 4.7 mJ, respectively.

The measured velocity at time 40 ± 10 ns after the breakdown was ∼780 m s^{-1}. Since bubble's wall velocity decreases rapidly, the velocity at 110 ± 20 ns after the

breakdown was ∼300 m s^{-1} (both values are not shown in figure 10 to avoid a lack of clarity), while at 40 μs after the breakdown the bubble's wall velocity is below 10 m s^{-1}. Results are in accordance with measurements based on shadow photography as reported by Vogel *et al* [2].

4. Conclusion

We have presented measurements of cavitation-bubble dynamics based on a laser beam-deflection probe (BDP). This method can be applied as an alternative to the widely used technique based on shadow photography. We used precise relative positioning of the breakdown region with respect to the probe beam as well as a relatively small diameter of the probe beam's waist. This allowed us to detect and analyse in detail the signal from the shock wave and the cavitation bubble. Four characteristic peaks due to probe-beam deflections resulting from a shock wave were detected. The last three of them correspond to known effects, like the high-pressure gradient of the shock front, the diverging lens effect and the presence of a rarefaction wave. However, the first one, we believe, corresponds to the beam reflection from the surface of the shock-wave front. This, to the best of our knowledge, is the first report of this effect.

The time evolution of the bubble and the shock-wave separation immediately after the optical breakdown as well as the first three oscillations of the cavitation bubble were presented. The described method, based on laser BDP, can be applied for measuring fast phenomena that follow immediately after laser-induced breakdown as well as the whole dynamics of the bubble oscillations corresponding to a three-orders-of-magnitude larger time scale.

References

[1] Kennedy P K 1995 A first-order model for computation of laser-induced breakdown thresholds in ocular and aqueous media: part I—theory *IEEE J. Quantum Elect.* **31** 2241–9

[2] Vogel A, Busch S and Parlitz U 1996 Shock wave emission and cavitation bubble generation by picosecond and nanosecond optical breakdown in water *J. Acoust. Soc. Am.* **100** 148–65

[3] Lauterborn W 1972 High-speed photography of laser-induced breakdown in liquids *Appl. Phys. Lett.* **21** 27–9

[4] Vogel A, Lauterborn W and Timm R 1989 Optical and acoustic investigations of the dynamics of laser-produced cavitation bubbles near a solid boundary *J. Fluid Mech.* **206** 299–338

[5] Kurz T, Kröninger D, Geisler R and Lauterborn W 2006 Optic cavitation in an ultrasonic field *Phys. Rev.* E **74** 066307

[6] Emmony D C, Geerken T and Klein-Baltink H 1983 Laser-generated high-frequency sound waves in water *J. Acoust. Soc. Am.* **73** 220–4

[7] Apitz I and Vogel A 2005 Material ejection in nanosecond Er:YAG laser ablation of water, liver, and skin *Appl. Phys.* A **81** 329–38

[8] Tomita Y and Shima A 1986 Mechanisms of impulsive pressure generation and damage pit formation by bubble collapse *J. Fluid Mech.* **169** 535–64

[9] Noack J, Hammer D X, Noojin G D, Rockwell B A and Vogel A 1998 Influence of pulse duration on mechanical effects after laser-induced breakdown in water *J. Appl. Phys.* **83** 7488–95

[10] Lauterborn W and Koch A 1987 Holographic observation of period-doubled and chaotic bubble oscillations in acoustic cavitation *Phys. Rev.* A **35** 1974–6

[11] Liu Z, Steckman G J and Psaltis D 2002 Holographic recording of fast phenomena *Appl. Phys. Lett.* **80** 731–3

[12] Petkovsek R, Mozina J and Mocnik G 2005 Optodynamic characterization of shock waves after laser-induced breakdown in water *Opt. Express* **13** 4107–12

[13] Lu J, Xu R Q, Chen X, Shen Z H, Ni X W, Zhang S Y and Gao C M 2004 Mechanisms of laser drilling of metal plates underwater *J. Appl. Phys.* **95** 3890–4

[14] Vogel A, Schweiger P, Frieser A, Asiyo M N and Bringruber R 1990 Intraocular Nd:YAG laser surgery: light–tissue interaction, damage range, and reduction of collateral effects *IEEE J. Quantum Elect.* **26** 2240–60

[15] Brujan E A and Vogel A 2006 Stress wave emission and cavitation bubble dynamics by nanosecond optical breakdown in a tissue phantom *J. Fluid Mech.* **558** 281–308

[16] Davidson G P and Emmony D C 1980 A schlieren probe method for the measurement of the refractive index profile of a shock wave in a fluid *J. Phys. E: Sci. Instrum.* **13** 92–7

[17] Diaci J 1992 Response functions of the laser beam deflection probe for detection of spherical acoustic waves *Rev. Sci. Instrum.* **63** 5306–10

[18] Diaci J and Mozina J 1995 Multiple-pass laser beam deflection probe for detection of acoustic and weak shock waves in fluids *Rev. Sci. Instrum.* **66** 4644–8

[19] Villagrán-Muniz M, Sobral H and Navarro-González R 2003 Shock and thermal wave study of laser-induced plasmas in air by the probe beam deflection technique *Meas. Sci. Technol.* **14** 614–8

[20] Diaci J and Mozina J 1996 Measurement of energy conversion efficiency during laser ablation by multiple laser beam deflection probe *Ultrasonics* **34** 523–5

[21] Petkovsek R, Babnik A and Diaci J 2006 Optodynamic monitoring of the laser drilling of through-holes in glass ampoules *Meas. Sci. Technol.* **17** 2828–34

[22] Docchio F, Regondi P, Capon M R C and Mellerio J 1988 Study of the temporal and spatial dynamics of plasmas induced in liquids by nanosecond Nd:YAG laser pulses: 2. Plasma luminescence and shielding *Appl. Opt.* **27** 3669–74

[23] Vogel A, Nahen K, Theisen D and Noack J 1996 Plasma formation in water by picosecond and nanosecond Nd:YAG laser pulses—part 1: optical breakdown at threshold and superthreshold irradiance *IEEE J. Sel. Top. Quant.* **2** 847–60

[24] Vogel A 2001 *Optical Breakdown in Water and Ocular Media, and Its Use for Intraocular Photodisruption* (Aachen, Germany: Shaker)